Applied Surface Science 614 (2023) 156211

Contents lists available at ScienceDirect

Applied Surface Science

journal homepage: www.elsevier.com/locate/apsusc

Full length article

Effect of interference laser treatment on the surface region homogeneity of a biomedical β-Ti alloy

D. Kuczyńska-Zemła [a,b,*], P. Kwaśniak [b], A. Sotniczuk [a], T. Boll [c], D. Chassaing [c], P. Bazarnik [a], P. Wieciński [d], M. Pisarek [e], R. Ostrowski [f], H. Garbacz [a]

[a] Faculty of Materials Science and Engineering, Warsaw University of Technology, Poland
[b] Multidisciplinary Research Centre, Cardinal Stefan Wyszynski University in Warsaw, Poland
[c] Karlsruhe Nano Micro Facility (KNMF), Karlsruhe Institute of Technology (KIT), Institute for Applied Materials (IAM-WK) and Institute for Nanotechnology (INT), Eggenstein-Leopoldshafen, Germany
[d] Faculty of Chemistry, Warsaw University of Technology, Warsaw, Poland
[e] Institute of Physical Chemistry, Polish Academy of Sciences, Warsaw, Poland
[f] Institute of Optoelectronics, Military University of Technology, Warsaw, Poland

ARTICLE INFO

Keywords:
Titanium alloy
Laser treatment
Surface
Direct Laser Interference Patterning
Atom probe tomography

ABSTRACT

This study provides a detailed insight into the microstructure and chemical composition of a surface region of a novel, metastable Ti-29Nb-13Ta-4.6Zr (TNTZ) alloy with a low Young's modulus modified by Direct Laser Interference Patterning (DLIP) using an Nd:YAG (1064 nm) with 10 ns pulse duration. Scanning Electron Microscopy (SEM), Transmission Electron Microscopy, and Scanning Transmission Electron Microscopy (STEM) were employed to investigate the microstructure of the cross-section of modified TNTZ. For chemical composition analysis of the surface region, X-ray Photoelectron Spectroscopy (XPS) and Atom Probe Tomography (APT) were applied. The chemical composition analysis was divided into two stages: surface analysis (XPS and APT) and analysis of a bulk (APT at the depth of 300 nm). Through the interference phenomenon during DLIP treatment, we observed significant microstructure evolution in the surface region of TNTZ alloy — grain refinement on the tops of the grooves while the microstructure at the bottoms was unattached. APT measurements at the depth of 300 nm revealed a noticeable local chemical heterogeneity of the substrate alloy, that has not been considered before when designing the metastable β-Ti systems. The applied laser treatment homogenizes the remelted zones and thus provides an additional factor influencing the surface properties.

1. Introduction

The global demand for higher quality medical devices has driven extensive investigation and development of novel biomaterials for various applications in the human body. The World Health Organization (WHO) identified the number of medical devices used in humans as 1.5 million individual devices each year [1]. It is predicted that by the end of 2030, the number of total hip replacements and total knee arthroplasties will increase by, respectively, 174% and 673% from the present rate [2–4]. Such a growing number indicates the necessity to design new long-term implantable devices with improved properties.

Analyzing the current state of knowledge, novel β titanium alloys [5,6], such as Ti-29Nb-13Ta-4.6Zr, are designed for orthopedic implants due to their excellent biocompatibility [7], improved corrosion resistance, and low elastic modulus compared to the standard Ti-based material [7,8]. These system designs are based on the electronic bond order, d-band energy level [9] or electron-to-atom ratio parameters [10,11], introduced to control the thermodynamic stability of the homogeneous body-centered cubic crystal lattice. Although such an approach has been confirmed to be efficient in the elaboration of new materials with desired properties, their atomic scale chemical homogeneity has not been intensively explored in the past.

However, despite described advantageous features, there are several crucial requirements for medical devices such as the condition of their surface. In terms of biomedical application surface properties, such as topography [12,13] and chemical composition [14,15], are the most important in the case of long-term, bone-implant anchoring. To further improve the bone-implant anchoring process and trigger cellular response, the surface of titanium prostheses can be modified by numerous mechanical, chemical, or other processes (*e.g.* physical) [14,16,17]. Cells are prone to surface irregularities and change their shape, orientation, and quantity depending on the implant surface [18,19].

* Corresponding author at: Multidisciplinary Research Centre, Cardinal Stefan Wyszynski University in Warsaw, Poland.
E-mail address: d.kuczynska-zemla@uksw.edu.pl (D. Kuczyńska-Zemła).

https://doi.org/10.1016/j.apsusc.2022.156211
Received 27 July 2022; Received in revised form 9 December 2022; Accepted 21 December 2022
Available online 24 December 2022

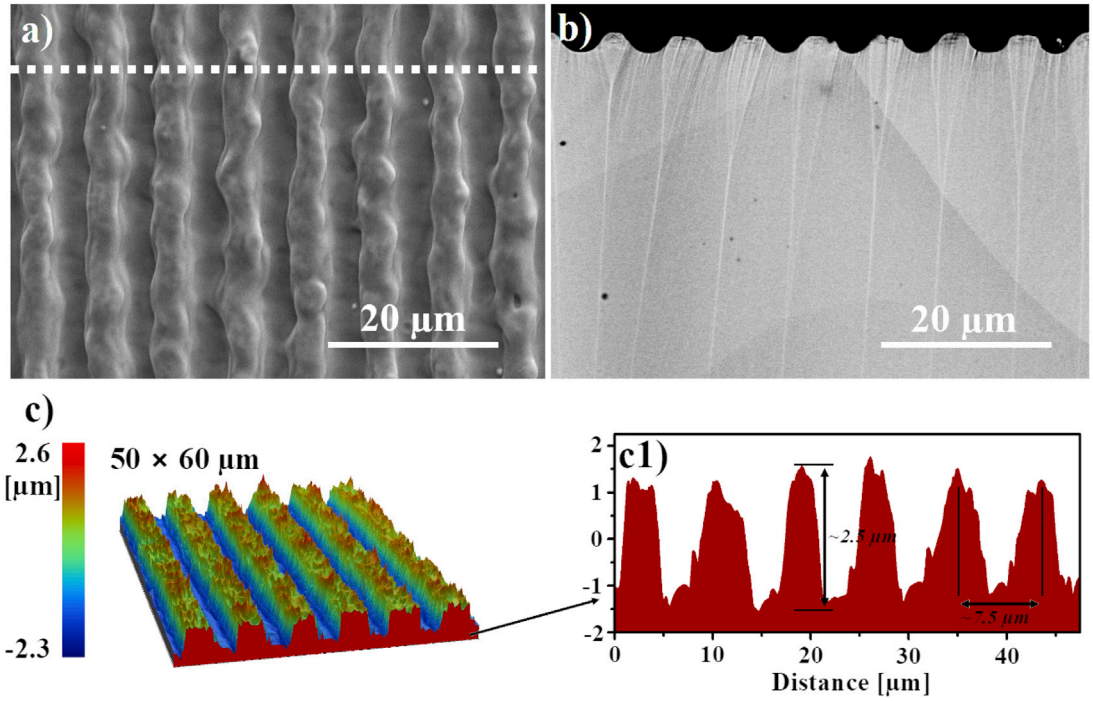

Fig. 1. Morphology of the TNTZ sample (a) with the corresponding cross-section (b), The dashed line schematically corresponds to the position where the cross-section was realized, topography of modified TNTZ (c) with the corresponding 1D profile (c1).

Compression of the cell nuclei and constraints on the cell body, both caused by surface topography, are reasons for cytoskeletal reorganization, which provoke specific cellular behaviors such as spreading and alignment. Topographic periodic structures force cells to accommodate and create intracellular architecture and signaling activities [20]. Specific cellular activities are dependent on the both type of cells and type of the patterns, their sizes, and geometries. When the cells adhere to periodic grooves, their bodies extend along the long axes of the groove and shows direct orientation [21]. According to the literature, microgrooves may promote osteogenic transition [22].

One of the promising techniques for producing diversified, periodic surface topographies is laser processing [15,18,23], especially Direct Laser Interference Patterning (DLIP) [24,25]. This single-step, contact-free and precise method benefits the biological properties of implantable devices, *i.e.*, due to the characteristic periodic pattern, DLIP-modified titanium improves cellular alignment [21,24].

DLIP treatment provides extremely high heating and cooling rates (for titanium temperatures exceeding >2350 °C [26]). In DLIP processing, melting of the material occurs mainly at maxima intensity positions [27–29] — the bottom sites of the grooves. The melted material is then transported by Marangoni convection to the minima intensity positions [30] — the top sites of the grooves. The non-uniform heating process during DLIP treatment necessitates analyzing those two places separately. Our previous studies showed that DLIP treatment of pure titanium caused grain refinement in the uppermost surface region [31] as well as changes in oxide layer composition [25], which may have a crucial effect on the resultant functional properties of the surface [32]. Moreover, other reports pointed out different oxide layers with the two mentioned sites (bottom, top) of the grooves [26,28,33]. Otherwise, it is known that the type of applied heat treatment has a fundamental impact on the structure and properties of metastable β-Ti alloys, including the TNTZ [34–38]. That is, laser surface treatment of β or near β type alloys causes, separately from surface structuring, microstructure [39] or phase transformation [40]. However, this aspect is not well documented with only a few reports not related to processing with the DLIP approach, in which the structuring mechanism is based on the interference phenomenon.

To provide new insights into the current understanding of laser texturing of the metastable β-Ti alloys, we present an in-depth analysis of the structure and chemical composition of DLIP-modified TNTZ alloy using complementary techniques. The phenomena occurring in the TNTZ substrate after DLIP treatment were analyzed on several scales: micro (optical profilometry and Scanning Electron Microscopy — SEM), nano (Scanning Transmission Electron Microscopy — STEM and Transmission Electron Microscopy — TEM), and atomic (Atom Probe Tomography — APT).

2. Methods

The microcrystalline β titanium alloy with the nominal composition Ti-29Nb-13Zr-4.6Zr (wt.%) was analyzed in this study. The TNTZ alloy was fabricated and processed at TIMET UK company. The considered alloy was hot forged at 1050 °C followed by hot rolling at 900 °C. The final solution treatment was performed at 950 °C for 30 min and then terminated with water quenching.

The DLIP treatment was performed under standard atmospheric pressure and air composition using a Nd:YAG laser (1064 nm) and a mirrored interferometer. Each sample was irradiated with three laser pulses using pulse energy of about 420 mJ and a pulse width of 10 ns. An exact specification of the DLIP treatment is presented in our previous studies [25]. Angle in-between two interfering beams during the experiments was 8.7°. The spot size in the performed experiments was in the range of 8–9 mm.

The morphology of the modified TNTZ sample was investigated in an SEM form Hitachi, SU-70. To precisely analyze the surface topography, optical profilometry with Wyko NT9300 was performed. In order to estimate surface roughness without waviness of the profile, the profiles were treated with the cut-off wavelength of 1.983 µm. Microstructural characterization was conducted on the cross-sections of the modified TNTZ sample. For SEM (Hitachi, SU8000) observations the TNTZ specimens were prepared by cutting the modified sample perpendicular to the long axis of the grooves and polishing the cross-sections using a Hitachi Ion Milling System IM-4000. Detailed microstructural analysis was carried out using a transmission electron

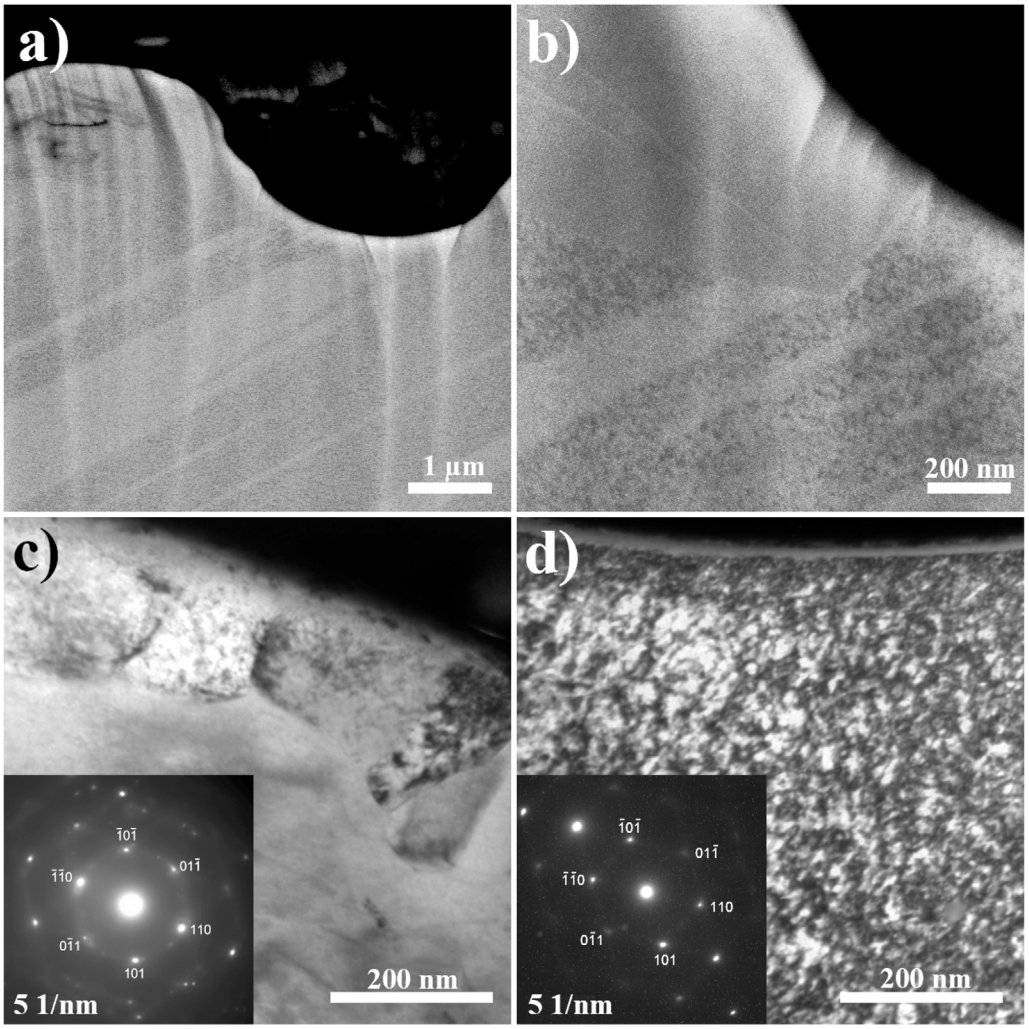

Fig. 2. Cross-sectional SEM images of the bottom and top positions (a) and with higher magnification at the region of interest (b), cross-sectional TEM images of the top (c) and bottom position (d), and corresponding SAED patterns. In SAED patterns, all the reflections presented come from a β phase.

microscope JEOL JEM 1200 operating at an accelerating voltage of 120 kV and CS-corrected dedicated Scanning Transmission Electron Microscope (STEM) Hitachi HD2700, operating at 200 kV. Samples for TEM or STEM observations were prepared using a Focused Ion Beam (FIB) Hitachi NB-5000 microscope. The lamellas were cut perpendicular to the laser-treated surface. STEM observations were carried out in Bright-Field (BF) and High-Angle Annular Dark-Field (HAADF) modes. For selected samples, Selected Area Electron Diffraction (SAED) patterns were obtained.

The analysis of the chemical composition of the surfaces of the produced samples was performed using a Microlab 350 (Thermo Electron) spectrometer with dual anode Al/Mg. For XPS analysis was used AlKα radiation: hν = 1486.6 eV, 300 W, 15 kV. Survey spectra and high-resolution XPS spectra were recorded with the hemispherical analyzer at the pass energy 100 and 40 eV, respectively. All XPS spectra were registered over a representative 2 × 5 mm surface area. The Avantage software ver. 59911 was used to evaluate the XPS data.

The tip samples for APT were prepared using a Zeiss Auriga Dual Beam FIB using Ga^+ ions. The region of interest was firstly protected by a magnetron sputtered layer of Ag. In order to avoid damage caused by the Ga^+ ion beam, a capping layer of Pt was put on the surface, as described by Larson et al. [41]. Atom probe acquisition was conducted in a Local Electrode Atom Probe (LEAP) Cameca 4000X HR under an ultra-high vacuum with the base temperature set to 50 K. The instrument automatically adjusts the standing high voltage to match the detection rate set to 0.5%. The device operated with laser pulsing with a pulse energy of 30 pJ and a pulse repetition rate of 100–200 kHz. The APT data were reconstructed and analyzed using the Cameca IVAS 3.6.14 software.

3. Results and discussion

3.1. Morphology and topography

Fig. 1 presents the morphology, cross-section, and topography of a DLIP-modified TNTZ sample. The examination displayed a well-defined and repeatable, grooved structure on the TNTZ surface (Fig. 1a). Notable is also the lack of cracks and delamination as well as discontinuities (Fig. 1b), which could negatively influence the biological or corrosion performance of modified surfaces. This emphasizes the beneficial features of the DLIP technique. The pulse energy of 420 mJ and triple exposition led to the creation of a periodic pattern with a period of approx. 7.5 µm and a height of 2.5 µm (Fig. 1c and c1). In terms of biomedical applications, cell behavior strongly depends on the groove's dimensions — depth and period [42]. It was reported that cells follow the physical pattern on the surface if the pattern is not greater than the size of the cell body [43,44]. According to the literature, the best grooves/patterns for osteoblasts alignment are in a range of 1–10 µm which indicates that the grooves on TNTZ may be promising in terms of the biological response. The value of surface roughness

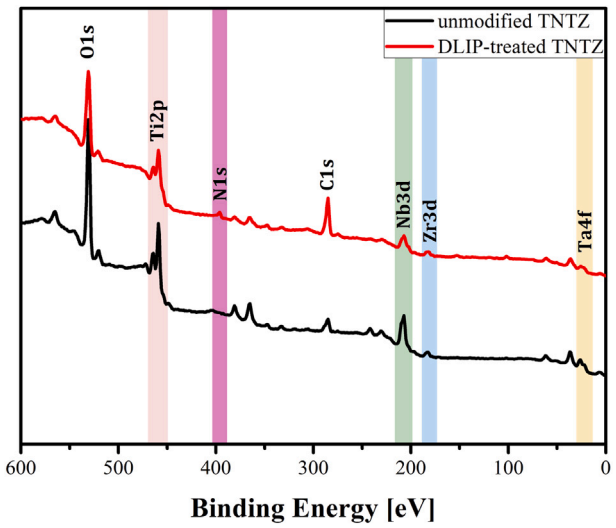

Fig. 3. Survey spectra of unmodified TNTZ and DLIP-treated TNTZ with the color distinction of main elements of the alloy. The main difference is the presence of N1s peak in DLIP-treated TNTZ.

(Ra — arithmetic average deviation of surface roughness) is 890 nm, which indicates a significant development of the TNTZ surface (in the polished state, Ra did not exceed a dozen nm [45] — Ra = 11 nm) (see supplementary Fig. 1). The roughness (Ra) with applied wavelength cut-off (without waviness of periodic profile) is much smaller, 144 nm. However, it is still higher than the polished TNTZ specimen, which indicates that DLIP treatment also results in nano-scale roughness.

The SEM cross-sections represent large (β) grains in the microstructure of the modified TNTZ substrate. Our previous studies showed that grain size is in the range of 90 μm [45] and the alloy is composed of a BCC β matrix and a small amount of an orthorhombic α'' martensite phase. The equalized shape of the grains indicates that the TNTZ microstructure is fully recrystallized. The local heating occurs at the maximum intensity positions (bottom). Marangoni convection transports the melted material to the minimum intensity positions (top). The result of this process is a periodic pattern. Moreover, non-uniform heating caused by the interference phenomenon may also induce local thermal reactions on titanium alloy surfaces and local reconstruction of the microstructure. To investigate these effects, detailed analyses of the cross-section were performed.

3.2. Microstructure

Detailed characterization of the microstructure was performed using complementary SEM and TEM techniques. The SEM micrographs in Fig. 2 (a) and (b) represents the interface between the top and bottom sites of the grooves. The microstructure of the bottom region is composed of lamellar grains with a continuous structure of boundaries up to the free surface. Since the TNTZ is a metastable system, its microstructure in the solution treated state is mainly composed of large β grains with a possible occurrence of orthorhombic α'' martensite laths, as shown in Fig. 1 and Fig. 2, respectively. The presence of lamellar/twin grains in the bottom region may indicate the occurrence of plastic deformation by the twinning mechanism due to stresses applied during laser treatment. Also, the lamellar/twin grains are oriented at an angle close to 45° to the laser beam direction. If the laser beam caused the presence of normal, compressive stresses in the bottom region, the maximum shear stresses – which induced plastic deformation – will be oriented at an angle of 45° to the laser beam and also to the surface. Thus, it can be assumed that lamellar grain may be formed by twinning due to the shear stress created during laser treatment. However, our previous studies [45,46] also indicate the presence of a lamellar grain in TNTZ alloy in the polished, unmodified state (see supplementary Fig. S2). Furthermore, the SEM micrographs showed a sharp boundary between two analyzed sites of the grooves — bottom and top. Detailed TEM analysis revealed, that the microstructure at the top site is formed from nanometric grains (Fig. 2c) which are not present at the bottom region (Fig. 2d). The microstructure transformation at the top region results from the rapid crystallization of displaced melted material from the bottom sites. The material removed in the liquid phase from the bottom sites of the grooves takes all the heat with it and exposes the unmelted material that is negligibly affected by heat. The SAED patterns of the bottom and top sites of the grooves indicate that there are no ω or α'' phase reflections observed and all the reflections presented come from a β phase.

A microstructural analysis indicates that there is no melting on the macro-scale and that the heat-affected zone is limited to the very top of the grooves. Nevertheless, we found heterogeneity and local microstructure fluctuations at the surface region of laser-modified TNTZ alloy with a spatial period of 7.5 μm. The top sites of the grooves exhibit refined grains with nanometric sizes, while at the bottom the microstructure remains unchanged. Equally important is the fact that there is a strong correlation between the microstructure including the resultant surface properties and its chemical composition. Therefore, a chemical composition analysis, with the distinction of laser intensity position, will be subsequently investigated in this article.

3.3. Chemical state of the surface and substrate material

Due to the fact that the DLIP treatment is essentially local and concerns the uppermost zone of the material, the experiments performed were focused on the oxide layer and the bulk material close to the free surface region.

3.3.1. Surface region

The chemical composition was first measured using the XPS method and revealed the presence of all alloying elements such as Ti2p, Nb3d, Zr3d, and Ta4f (Fig. 3) for both analyzed states — unmodified TNTZ and DLIP-treated. A detailed analysis showed that the main components of the passive layer for both states are oxides of titanium, niobium, tantalum, and zirconium — TiO_2, Nb_2O_5, Ta_2O_5 and ZrO_2, which is consistent with previous reports [45,47]. Other oxides with a reduced amount of all alloying elements were also detected but in smaller amounts.

In addition, there is a strong peak around 396.0 eV which can be attributed to the nitrogen that forms the titanium nitride phase or is implemented in the structure of the titanium oxide. Our previous studies concerning DLIP treatment of titanium [26] demonstrated that a nitride phase is located between the oxide layer and titanium matrix. This nitride may have an influence on the surface properties of the modified TNTZ. There can also be a different distribution of oxides species in the laser-irradiated TNTZ compared to the unmodified sample, as presented in laser-patterned steel [33]. Therefore, laser-patterned TNTZ substrate analysis was performed and compared to the unmodified state using Atom Probe Tomography.

APT was used for quantitative compositional analysis. Fig. 4 displays concentration heat maps and concentrations of different elements for the surface region of the top and bottom sites of the grooves of the laser-modified TNTZ and the unmodified TNTZ. There are two specific sections, an O-rich zone located directly below the free surface; and a deeper N-rich region.

A comparison of the O-rich region for all states showed the highest oxygen content for the unmodified material. Both laser states indicate a lower O concentration, which suggests a reconstruction of the oxide layer during DLIP processing takes place. Moreover, the amount of alloying elements (Ti, Nb, Ta, and Zr) is similar for all samples. Another significant output of the experiments is related to the increased nitrogen

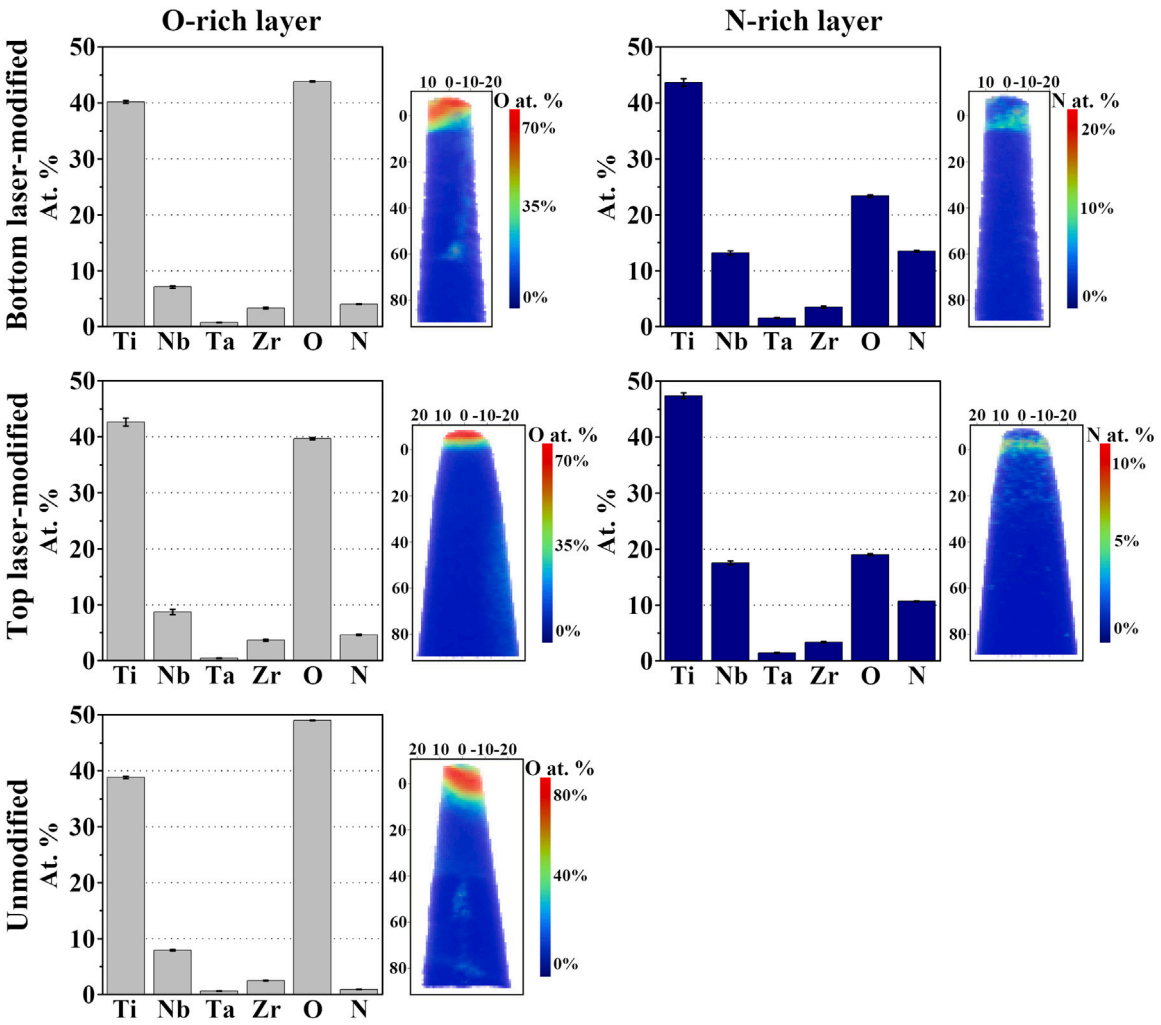

Fig. 4. Chemical composition of laser-treated TNTZ obtained from APT reconstruction with a distinction of laser intensity position and reference to the unmodified state. Atom heat maps present the location of each layer. For each layer, a volume with fixed isosurfaces was created and chemical compositions correspond to those volumes. For the bottom of the grooves, the concentration values for the O-rich and N-rich regions were constructed as 46.6% of O and 8.3% of N, while for the top 40.4% of O and 7.4% of N. For the unmodified state, only an oxygen-rich layer can be distinguished and the concentration was determined to be 40.6% of O. The concentration values were similar between the APT tips for each of the groove sites as well as the unmodified TNTZ. The size of the tips was 50 × 50 × 100 nm.

fraction in the laser-treated states compared to those of the unmodified alloy. The chemical composition of the unmodified alloy demonstrates a small amount of nitrogen in the O-rich layer, while for both laser-patterned positions the nitrogen content is much higher. The above findings agree with available literature reporting an increased amount of nitrogen after laser treatment of a titanium substrate [24,48,49]. The highest nitrogen level was detected at the bottom of the grooves of the laser-treated TNTZ alloy, which is connected to the highest operating temperature at this place.

The N-rich layer, at both laser intensity positions, exhibits an increased concentration of niobium and tantalum, while other alloying elements (Ti, Zr) remain on a similar level as in the O-rich layer. From the results, it is evident that the increased concentration of Nb and Ta can be attributed to the increased concentration of nitrogen and there is no pronounced depletion of these elements near the N-rich regions. The possible explanation for the chemical composition variation is the fact that Ti is the dominant metal in alloys which easily forms both oxide and nitride compounds. Looking at the binary phase diagrams of Nb–N, Nb–O, Ta–N and Ta–O one can observe that the melting/crystallization points (T_M) of Nb_X-N_Y ($T_M \approx 2430$ °C for Nb_2N) and Ta_X-N_Y ($T_M \approx 3150$ °C for TaN) are always higher than the corresponding temperature of Nb_X-O_Y ($T_M \approx 2200$-2250 °C for NbO and NbO_2) and Ta_X-O_Y ($T_M \approx 1550$ °C for Ta_2O_5) [50]. Based on these data, probably during rapid heating to the temperatures close to melting point of the alloy, Nb_X-N_Y and Ta_X-N_Y are thermodynamically preferred to form which is visible in the APT measurements.

We did not observe any differences in oxide layer thickness between the analyzed states, which may be related to the parameters of the laser processing. Although in the literature a periodically modulated thickness of the oxide layer for pure titanium [26], aluminum [29] or steel [33] was observed, our TNTZ alloy is composed of four alloying elements and oxidation and nitridation processes may occur differently or competitively.

3.3.2. Composition and homogeneity of the substrate alloy

Interestingly, at the bottom position as well as for unmodified TNTZ, a trace amount of oxygen was found within the bulk material necessitating additional analysis. To perform a precise chemical analysis with the atomic resolution of the composition of our TNTZ alloy, a fixed cylinder with a height of 15 nm and diameter of 50 nm was selected from each probed volume in the core of the reconstructed tips at a depth of 300 nm. These selected datasets reduce the area of analysis and eliminate the influence of the shank surface region, which experienced some Ga implantation during the FIB preparation of the tip. The composition of the unmodified state and the laser-treated samples are similar and in good agreement with the nominal composition of Ti-20.2Nb-4.6Ta-3.3Zr in at.%, as shown in Table 1.

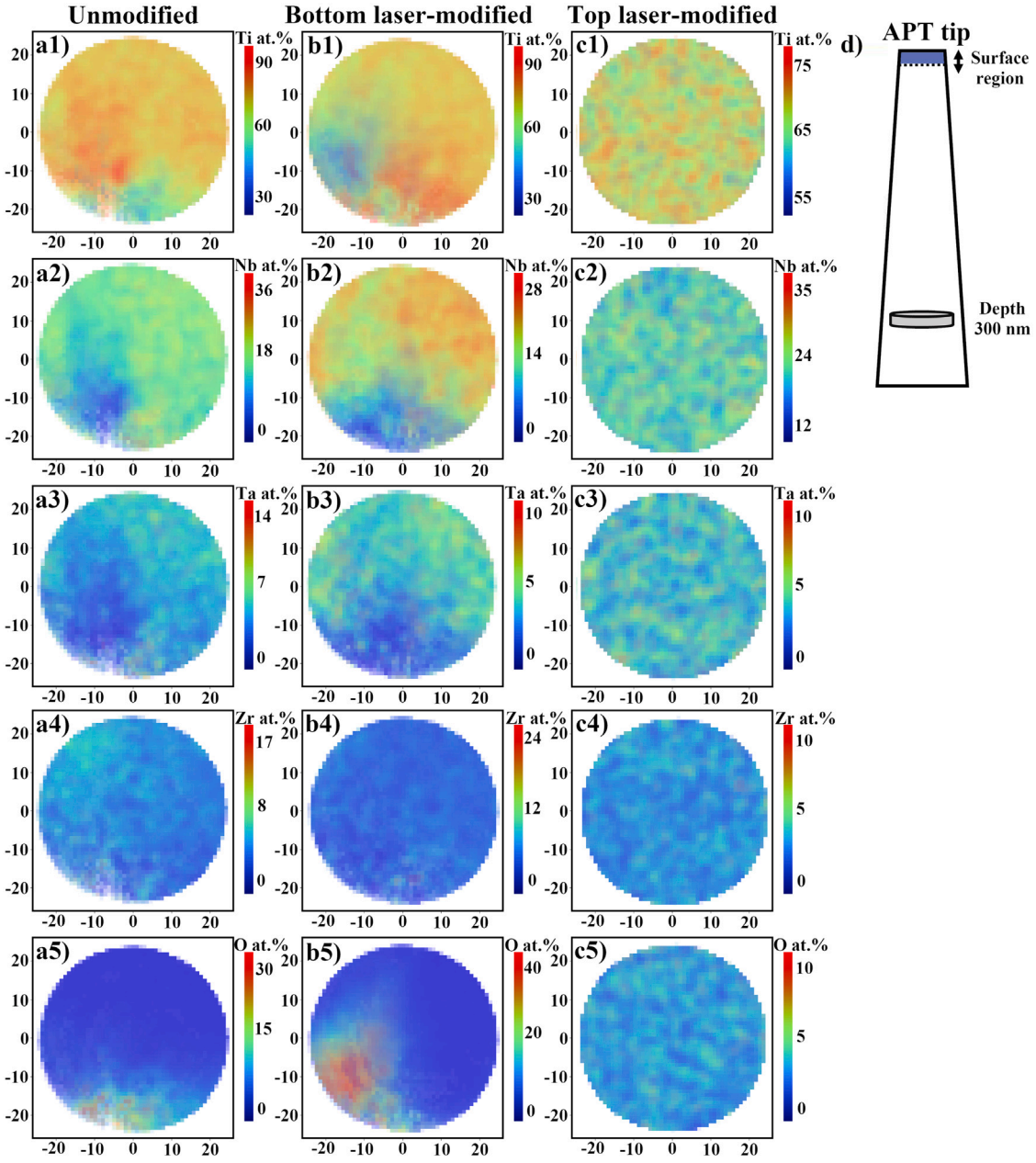

Fig. 5. Heat maps of cylinders slices aligned in the xy-plane; Alloying elements (Ti, Nb, Ta, and Zr) and oxygen for the unmodified state (a1–a5) and both laser intensity positions — bottom (b1–b5) and top (c1–c5). The cylinder slice for each heat map is 15 nm high with a 50 nm diameter; (d) a schematic representation of the analysis site.

Table 1
Elemental concentrations in at.%, measured by APT. Hydrogen was excluded from further evaluation due to the presence of residual hydrogen gas in the chamber.

	Unmodified	Bottom	Top
Ti	69.7	68.3	69.1
Nb	15.8	16.2	19.2
Ta	3.2	3.4	3.9
Zr	3.6	3.3	3.2
O	2.0	3.8	2.3
N	0.7	1.0	0.9

Fig. 5 shows heat maps of thin slices of the cylinder displaying the lateral distributions of Ti, Nb, Ta, and Zr concentrations within the microstructure of the bulk material. Within the top site of the groove, the distribution of all alloying elements as well as oxygen is fairly homogeneous (Fig. 5), while at the bottom site and for the unmodified state alloying elements, lateral oxygen distribution exhibits visible segregation. In both mentioned states (unmodified and bottom), titanium-rich regions overlap with the oxygen-rich and niobium-depleted fields, respectively. Another noticeable segregation effect can be observed for Ta, which preferentially occupies the Nb-saturated part of the material. It should be noted that the variation of the local concentration of alloying elements is pronounced reaching an amplitude level of tens of atomic percent. The presented chemical inhomogeneity of the unmodified and bottom state can be justified on the basis of the Friedel model of the electronic structure of transition metals [51]. The cohesive energy of these elements at the BCC structure increases with an increasing number of *d*-type valence electrons, reaching its maximum at the half filled *d*-band. Nb and Ta have a larger number of *d*-type electrons than

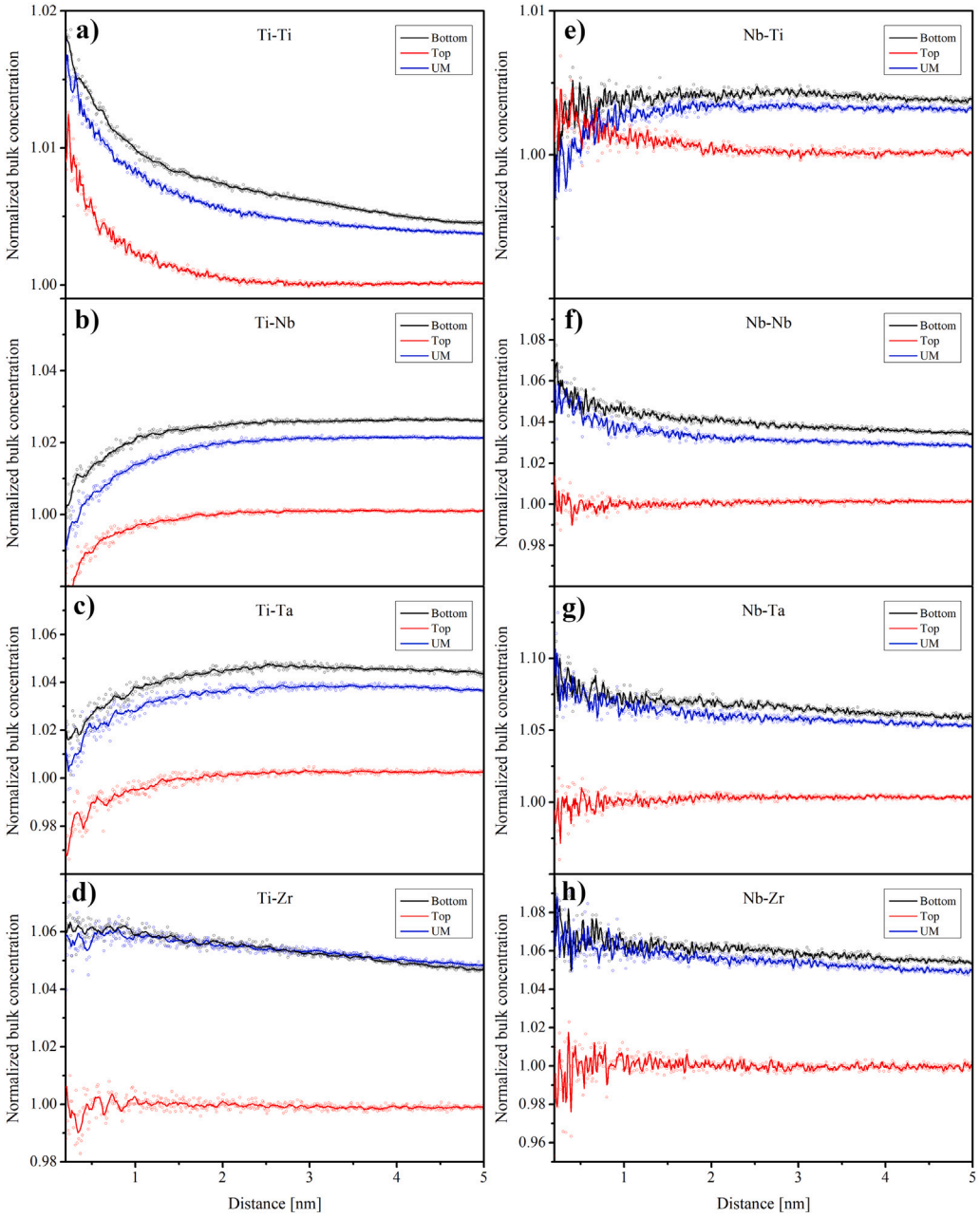

Fig. 6. Ti-centered (a–d) and Nb-centered (e–h) partial radial distribution function (RDF) vs. radial distance for the unmodified state and both laser intensity positions. Partial RDF = 1, describes a perfectly random solid-solution distribution. For plotting RDF graphs the ROI cylinder is 100 nm long with a 50 nm diameter. Open circles describe actual results while the solid line is an approximation. Bottom labels (black) refer to maximum intensity position, top minimum (red) and UM (blue) to unmodified state of TNTZ alloy.

Ti, thus, acting as β stabilizers, also providing also more binding states and leading to strong Nb–Nb, Ta–Ta, and Nb–Ta attraction.

The gathered results reveal that although the adopted heat treatment of TNTZ includes rapid, water quenching from a high temperature (950 °C), and stable β phase, it does not imply, a truly, atomic-scale, disordered configuration of the alloy. The presented, evident gradient of chemical composition results in serious repercussions in terms of the homogeneity of the properties and structural stability of the investigated system. In general, the metastable β-Ti alloys are designed mainly based on the two electronic criteria: (i) the average e/a electron to atom ratio [52] and (ii) the average Bo bond order and Md d-band energy level [53]. Small changes of these parameters lead to crucial changes of both, the mechanical properties [4,54] and structural stability of the alloy, *e.g.* an increase of e/a by 0.4 increases the Young modulus by approx. 35% [4,55,56] or transforms the quenched β phase to $\beta + \alpha'' + \omega$ mixtures [52]. According to Fig. 5, high chemical homogeneity is achieved on top of the grooves formed from the liquid phase during the DLIP process. This observation directly indicates that apart from the topography and microstructural changes, the studied laser treatment introduces another essential material transformation: local chemical homogenization.

A radial distribution functions (RDFs) analysis of the atom probe data for the TNTZ before and after laser treatment are presented on Fig. 6. The unity value in RDF relates to the perfectly random distribution, while any deviation from unity is related to the clustering or ordering processes [57]. The step size of the calculated RDF in the investigated region of interest (ROI) was equal to 0.01 nm. The RDFs were obtained by plotting the bulk-normalized concentration as a function of distance from the Ti and Nb center for the ROI of a cylinder

with a height of 100 nm and a diameter of 50 nm at a depth of 300 nm in the reconstructed tips.

A RDF analysis of the atom probe data reveals a tendency for chemical clustering/segregation for the TNTZ before laser treatment (Fig. 6) [57–62]. Moreover, it has been found that laser treatment has no evident effect on the material at the intensity maxima (bottom sites). On the other hand, top sites of the grooves exhibit more random distribution of alloying elements indicating that DLIP process increases chemical homogeneity of the alloy in these regions. Although some increase in Ti–Ti binding and depletion in Ti–Nb, Ti–Ta clusters is visible in all cases, provided the RDF curves confirm that the remelted, top zones of the grooves are more chemically homogeneous than the bottom sites or unmodified material. In general, the most noticeable attraction exists for Nb–Nb and Nb–Ta pairs as these elements possess more d-type electrons leading to a larger amount of available bonding states. Local clustering of the above elements is much weaker on top of the grooves implying more uniform distribution of alloying elements of this state as shown in Fig. 5. Finally, as the valence structure of Zr is close to those of Ti, the propensity of Zr to segregate is less pronounced than that of Nb or Ta.

Our results indicate that due to the rapid crystallization of the liquid phase on top sites of the grooves, a pronounced chemical homogenization can be obtained along with grain refinement. Moreover, the observed local segregation of alloying elements in the solution-treated TNTZ alloy reveals that the metastable, biomedical Ti alloys also display an atomic scale gradient of mechanical properties and stability of the β-phase.

4. Conclusions

This paper presents direct experimental evidence for the microstructural and compositional evolution within the β TNTZ alloy after DLIP treatment. Laser processing was applied to fabricate well-defined and controlled periodic patterns on the surface of the TNTZ alloy. Applied laser processing parameters allow us to create grooves with a period of 7.5 μm and a height of 2.5 μm, which may be promising in the case of osseointegrating implants. The surface structuring mechanism, during DLIP modification, is based on the interference phenomenon which implies microstructural changes depending on the position of laser intensity. Our main findings are as follows:

- The obtained results confirmed that the DLIP treatment has an impact on the surface region of TNTZ alloy. This entails the fluctuating nature of the local microstructure and chemical composition of surface and bulk resulting from an interference phenomenon. This DLIP treatment promotes the formation of refined grains at the top sites of the grooves, while at the bottom the microstructure is comparable to that of unmodified TNTZ.
- Laser treatment also caused the formation of a well-defined layered structure of oxide- and nitride-enriched zones in the uppermost surface of TNTZ. The higher temperature at the maximum intensity position results in higher nitrogen content for the N-rich layer. Within the N-rich layer, a significant increase in niobium and tantalum content suggests a reaction with nitrogen.
- A homogenization of the chemical composition within the top sites of the grooves is proven by atom probe tomography and the resulting partial radial distribution functions (RDFs). Despite the fact that there is no evidence for microstructural transformation at the nanometer scale at the maximum intensity position, significant chemical distribution alterations at the atomic scale can be observed.

Declaration of competing interest

The authors declare that they have no known competing financial interests or personal relationships that could have appeared to influence the work reported in this paper.

Data availability

Data will be made available on request.

Acknowledgments

Our research was funded by POB Technologie Materiałowe of Warsaw University of Technology within the Excellence Initiative: Research University (IDUB), Poland programme. This work was partly carried out with the support of the Karlsruhe Nano Micro Facility (KNMFi, Germany, www.knmf.kit.edu), a Helmholtz Research Infrastructure at Karlsruhe Institute of Technology (KIT, www.kit.edu).

Donata Kuczyńska-Zemła also acknowledges the Foundation for Polish Science (FNP), Poland for their support in her career through the Start 2021 program.

Roman Ostrowski would like to acknowledge the university research grant, Military University of Technology, Poland, grant No. UGB/22-833/2021/WAT. The authors are also very grateful to Antoni Rycyk, who sadly passed away, for his contribution to the laser treatment methodology.

Appendix A. Supplementary data

Supplementary material related to this article can be found online at https://doi.org/10.1016/j.apsusc.2022.156211.

References

[1] I. Kulinets, Biomaterials and their applications in medicine, Regulatory Affairs for Biomaterials and Medical Devices, Woodhead Publishing Limited, 2015, pp. 1–10, http://dx.doi.org/10.1533/9780857099204.1.

[2] M. Geetha, A.K. Singh, R. Asokamani, A.K. Gogia, Ti based biomaterials, the ultimate choice for orthopaedic implants – a review, Prog. Mater. Sci. 54 (3) (2009) 397–425, http://dx.doi.org/10.1016/j.pmatsci.2008.06.004.

[3] S. Kurtz, K. Ong, E. Lau, F. Mowat, M. Halpern, Projections of primary and revision hip and knee arthroplasty in the United States from 2005 to 2030, J. Bone Joint Surgery - Series A 89 (4) (2007) 780–785, http://dx.doi.org/10.2106/JBJS.F.00222.

[4] P. Kwasniak, J.S. Wróbel, H. Garbacz, Origin of low Young modulus of multi-component, biomedical Ti alloys - seeking optimal elastic properties through a first principles investigation, J. Mech. Behav. Biomed. Mater. 88 (March) (2018) 352–361, http://dx.doi.org/10.1016/j.jmbbm.2018.08.040.

[5] B.Q. Li, R.Z. Xie, X. Lu, Microstructure, mechanical property and corrosion behavior of porous Ti–Ta–Nb–Zr, Bioact. Mater. 5 (3) (2020) 564–568, http://dx.doi.org/10.1016/j.bioactmat.2020.04.014.

[6] C. Mao, W. Yu, M. Jin, Y. Wang, X. Shang, L. Lin, X. Zeng, L. Wang, E. Lu, Mechanobiologically optimized Ti–35Nb–2Ta–3Zr improves load transduction and enhances bone remodeling in tilted dental implant therapy, Bioact. Mater. 16 (March) (2022) 15–26, http://dx.doi.org/10.1016/j.bioactmat.2022.03.005.

[7] M. Niinomi, M. Nakai, J. Hieda, Development of new metallic alloys for biomedical applications, Acta Biomater. 8 (11) (2012) 3888–3903, http://dx.doi.org/10.1016/j.actbio.2012.06.037.

[8] A. Sotniczuk, D. Kuczyńska-Zemła, P. Kwaśniak, M. Thomas, H. Garbacz, Corrosion behavior of Ti-29Nb-13Ta-4.6Zr and commercially pure Ti under simulated inflammatory conditions – comparative effect of grain refinement and non-toxic β phase stabilizers, Electrochim. Acta 312 (2019) 369–379, http://dx.doi.org/10.1016/j.electacta.2019.04.138.

[9] D. Kuroda, M. Niinomi, M. Morinaga, Y. Kato, T. Yashiro, Design and mechanical properties of new β type titanium alloys for implant materials, Mater. Sci. Eng., A 243 (1) (1998) 244–249, http://dx.doi.org/10.1016/S0921-5093(97)00808-3.

[10] E.W. Collings, J.C. Ho, R.I. Jaffee, Superconducting transition temperature, lattice instability, and electron-to-atom ratio in transition-metal binary solid solutions, Phys. Rev. B 5 (11) (1972) 4435–4449, http://dx.doi.org/10.1103/PhysRevB.5.4435.

[11] E.W. Collings, H.L. Gegel, A physical basis for solid-solution strengthening and phase stability in alloys of titanium, Scr. Metall. 7 (5) (1973) 437–443, http://dx.doi.org/10.1016/0036-9748(73)90092-6.

[12] L.C. Zhang, L.Y. Chen, L. Wang, Surface modification of titanium and titanium alloys: Technologies, developments, and future interests, Adv. Eng. Mater. 22 (5) (2020) 1–37, http://dx.doi.org/10.1002/adem.201901258.

[13] P. Jiang, Y. Zhang, R. Hu, X. Wang, Y. Lai, G. Rui, C. Lin, Hydroxyapatite-modified micro/nanostructured titania surfaces with different crystalline phases for osteoblast regulation, Bioact. Mater. 6 (4) (2021) 1118–1129, http://dx.doi.org/10.1016/j.bioactmat.2020.10.006.

[14] S. Bauer, P. Schmuki, K. Von Der Mark, J. Park, Engineering biocompatible implant surfaces Part I : Materials and surfaces, Prog. Mater. Sci. 58 (3) (2013) 261–326, http://dx.doi.org/10.1016/j.pmatsci.2012.09.001.

[15] S.H. Um, J. Lee, I.S. Song, M.R. Ok, Y.C. Kim, H.S. Han, S.H. Rhee, H. Jeon, Regulation of cell locomotion by nanosecond-laser-induced hydroxyapatite patterning, Bioact. Mater. 6 (10) (2021) 3608–3619, http://dx.doi.org/10.1016/j.bioactmat.2021.03.025.

[16] O. Unal, A. Cahit Karaoglanli, R. Varol, A. Kobayashi, Microstructure evolution and mechanical behavior of severe shot peened commercially pure titanium, Vacuum 110 (2014) 202–206, http://dx.doi.org/10.1016/j.vacuum.2014.08.004.

[17] C. Wedemeyer, H. Jablonski, A. Mumdzic-Zverotic, H. Fietzek, T. Mertens, G. Hilken, C. Krüger, A. Wissmann, H. Heep, R. Schlepper, M.D. Kauther, Laser-induced nanostructures on titanium surfaces ensure osseointegration of implants in rabbit femora, Materialia 6 (February) (2019) 100266, http://dx.doi.org/10.1016/j.mtla.2019.100266.

[18] V. Dumas, A. Guignandon, L. Vico, C. Mauclair, X. Zapata, M.T. Linossier, W. Bouleftour, J. Granier, S. Peyroche, J. Dumas, H. Zahouani, A. Rattner, Femtosecond laser nano / micro patterning of titanium influences mesenchymal stem cell adhesion and commitment, Biomed. Mater. 10 (2015) 055002, http://dx.doi.org/10.1088/1748-6041/10/5/055002.

[19] E.G. Long, M. Buluk, M.B. Gallagher, J.M. Schneider, J.L. Brown, Human mesenchymal stem cell morphology, migration, and differentiation on micro and nano-textured titanium, Bioact. Mater. 4 (March 2019) (2019) 249–255, http://dx.doi.org/10.1016/j.bioactmat.2019.08.001.

[20] N.A. Mohd Razali, W.C. Lin, N.A. Norzain, Z.W. Yu, Controlling cell elongation and orientation by using microstructural nanofibre scaffolds for accelerating tissue regeneration, Mater. Sci. Eng. C 128 (July) (2021) 112321, http://dx.doi.org/10.1016/j.msec.2021.112321.

[21] D. Kuczyńska-Zemła, E. Kijeńska-Gawrońska, M. Pisarek, P. Borowicz, W. Swieszkowski, H. Garbacz, Effect of laser functionalization of titanium on bioactivity and biological response, Appl. Surf. Sci. 525 (April) (2020) 146492, http://dx.doi.org/10.1016/j.apsusc.2020.146492.

[22] V. Dumas, A. Rattner, L. Vico, E. Audouard, J.C. Dumas, P. Naisson, P. Bertrand, Multiscale grooved titanium processed with femtosecond laser influences mesenchymal stem cell morphology, adhesion, and matrix organization, J. Biomed. Mater. Res. A 100 (11) (2012) 3108–3116, http://dx.doi.org/10.1002/jbm.a.34239.

[23] I.V. Smirnov, J.V. Rau, M. Fosca, A. de Bonis, A. Latini, R. Teghil, V.I. Kalita, A.Y. Fedotov, S.V. Gudkov, A.E. Baranchikov, V.S. Komlev, Structural modification of titanium surface by octacalcium phosphate via pulsed laser deposition and chemical treatment, Bioact. Mater. 2 (2) (2017) 101–107, http://dx.doi.org/10.1016/j.bioactmat.2017.03.002.

[24] C. Zwahr, D. Günther, T. Brinkmann, N. Gulow, S. Oswald, M.G. Holthaus, A.F. Lasagni, Laser surface pattering of titanium for improving the biological performance of dental implants, Adv. Healthcare Mater. 1600858 (2017) 1–9, http://dx.doi.org/10.1002/adhm.201600858.

[25] D. Kuczyńska, P. Kwaśniak, M. Pisarek, P. Borowicz, H. Garbacz, Influence of surface pattern on the biological properties of Ti grade 2, Mater. Charact. 135 (2018) 337–347, http://dx.doi.org/10.1016/j.matchar.2017.09.024.

[26] D. Kuczyńska-Zemła, G. Sundell, M. Zemła, M. Andersson, H. Garbacz, The distribution of O and N in the surface region of laser-patterned titanium revealed by atom probe tomography, Appl. Surf. Sci. 562 (May) (2021) 150193, http://dx.doi.org/10.1016/j.apsusc.2021.150193.

[27] M. Bieda, C. Schmädicke, T. Roch, A. Lasagni, Ultra-low friction on 100Cr6-steel surfaces after direct laser interference patterning, Adv. Eng. Mater. 17 (1) (2015) 102–108, http://dx.doi.org/10.1002/adem.201400007.

[28] M. D'Alessandria, F. Mücklich, Tailoring the chemical behavior of aluminum for selective etching by laser interference metallurgy, Appl. Phys. A 98 (2) (2010) 311–320, http://dx.doi.org/10.1007/s00339-009-5398-5.

[29] M. D'Alessandria, A. Lasagni, F. Mucklich, Direct micro-patterning of aluminum substrates via laser interference metallurgy, Appl. Surf. Sci. 255 (2008) 3210–3216, http://dx.doi.org/10.1016/j.apsusc.2008.09.018.

[30] R. Vilar (Ed.), Laser surface modification of biomaterials techniques and applications, Woodhead Publisher Elsevier, Woodhead Publishing, 2016, http://dx.doi.org/10.1016/B978-0-08-100883-6.00006-X.

[31] D. Kuczyńska-Zemła, P. Kwaśniak, A. Sotniczuk, M. Spychalski, P. Wieciński, J. Zdunek, R. Ostrowski, H. Garbacz, Microstructure and mechanical properties of titanium subjected to direct laser interference lithography, Surf. Coat. Technol. 364 (2019) 369–379, http://dx.doi.org/10.1016/j.surfcoat.2019.02.026.

[32] D. Kuczyńska-Zemła, A. Sotniczuk, M. Pisarek, A. Chlanda, H. Garbacz, Corrosion behavior of titanium modified by direct laser interference lithography, Surf. Coat. Technol. 418 (April) (2021) 127219, http://dx.doi.org/10.1016/j.surfcoat.2021.127219.

[33] A. Rosenkranz, L. Reinert, C. Gachot, H. Aboufadl, S. Grandthyll, K. Jacobs, F. Müller, F. Mücklich, Oxide formation, morphology, and nanohardness of laser-patterned steel surfaces, Adv. Eng. Mater. 17 (8) (2015) 1234–1242, http://dx.doi.org/10.1002/adem.201400487.

[34] M. Nakai, M. Niinomi, T. Oneda, Improvement in fatigue strength of biomedical β-type Ti-Nb-Ta-Zr alloy while maintaining low young's modulus through optimizing ω-phase precipitation, Metallur. Mater. Trans. A 43 (1) (2012) 294–302, http://dx.doi.org/10.1007/s11661-011-0860-3.

[35] T. Saito, T. Furuta, J.H. Hwang, S. Kuramoto, K. Nishino, N. Suzuki, R. Chen, A. Yamada, K. Ito, Y. Seno, T. Nonaka, H. Ikehata, N. Nagasako, C. Iwamoto, Y. Ikuhara, T. Sakuma, Multifunctional alloys obtained via a dislocation-free plastic deformation mechanism, Science 300 (5618) (2003) 464–467, http://dx.doi.org/10.1126/science.1081957.

[36] M. Tane, T. Nakano, S. Kuramoto, M. Hara, M. Niinomi, N. Takesue, T. Yano, H. Nakajima, Low Young's modulus in Ti-Nb-Ta-Zr-O alloys: Cold working and oxygen effects, Acta Mater. 59 (18) (2011) 6975–6988, http://dx.doi.org/10.1016/j.actamat.2011.07.050.

[37] T. Akahori, M. Niinomi, H. Fukui, M. Ogawa, H. Toda, Improvement in fatigue characteristics of newly developed beta type titanium alloy for biomedical applications by thermo-mechanical treatments, Mater. Sci. Eng. C 25 (3) (2005) 248–254, http://dx.doi.org/10.1016/j.msec.2004.12.007.

[38] M. Niinomi, M. Nakai, M. Hendrickson, P. Nandwana, T. Alam, D. Choudhuri, R. Banerjee, Influence of oxygen on omega phase stability in the Ti-29Nb-13Ta-4.6Zr alloy, Scr. Mater. 123 (2016) 144–148, http://dx.doi.org/10.1016/j.scriptamat.2016.06.027.

[39] T. Zhang, Q. Fan, X. Ma, W. Wang, K. Wang, P. Shen, J. Yang, L. Wang, Effect of laser remelting on microstructural evolution and mechanical properties of Ti-35Nb-2Ta-3Zr alloy, Mater. Lett. 253 (2019) 310–313, http://dx.doi.org/10.1016/j.matlet.2019.06.105.

[40] Y. Li, Y. Ding, K. Munir, J. Lin, M. Brandt, A. Atrens, Y. Xiao, J.R. Kanwar, C. Wen, Novel β-Ti35Zr28Nb alloy scaffolds manufactured using selective laser melting for bone implant applications, Acta Biomater. 87 (2019) 273–284, http://dx.doi.org/10.1016/j.actbio.2019.01.051.

[41] D.J. Larson, T.J. Prosa, R.M. Ulfig, B.P. Geiser, T.F. Kelly, Local Electrode Atom Probe Tomography, 2013, http://dx.doi.org/10.1007/978-1-4614-8721-0.

[42] K. Anselme, M. Bigerelle, B. Noël, A. Iost, P. Hardouin, Effect of grooved titanium substratum on human osteoblatic cell adhesion, Eur. Cells Mater. 1 (SUPPL. 2) (2001) 66.

[43] S. Ber, G. Torun Köse, V. Hasirci, Bone tissue engineering on patterned collagen films: An in vitro study, Biomaterials 26 (14) (2005) 1977–1986, http://dx.doi.org/10.1016/j.biomaterials.2004.07.007.

[44] X.F. Walboomers, H.J. Croes, L.A. Ginsel, J.A. Jansen, Growth behavior of fibroblasts on microgrooved polystyrene, Biomaterials 19 (20) (1998) 1861–1868, http://dx.doi.org/10.1016/S0142-9612(98)00093-3.

[45] D. Kuczyńska-Zemła, E. Kijeńska-Gawrońska, A. Chlanda, A. Sotniczuk, M. Pisarek, K. Topolski, W. Swieszkowski, H. Garbacz, Biological properties of a novel β-Ti alloy with a low Young's modulus subjected to cold rolling, Appl. Surf. Sci. 511 (October 2019) (2020) 145523, http://dx.doi.org/10.1016/j.apsusc.2020.145523.

[46] A. Sotniczuk, K. Majchrowicz, D. Kuczyńska-Zemła, M. Pisarek, B. Adamczyk-Cieślak, H. Garbacz, Surface properties and mechanical performance of Ti-based dental materials: Comparative effect of valve alloying elements and structural defects, Metallur. Mater. Trans. A 53 (1) (2022) 225–239, http://dx.doi.org/10.1007/s11661-021-06515-y.

[47] Y. Tanaka, M. Nakai, T. Akahori, M. Niinomi, Y. Tsutsumi, H. Doi, T. Hanawa, Characterization of air-formed surface oxide film on Ti-29Nb-13Ta-4.6Zr alloy surface using XPS and AES, Corros. Sci. 50 (8) (2008) 2111–2116, http://dx.doi.org/10.1016/j.corsci.2008.06.002.

[48] F. Torrent, L. Lavisse, P. Berger, J.M. Jouvard, H. Andrzejewski, G. Pillon, S. Bourgeois, M.C. Marco De Lucas, Wavelength influence on nitrogen insertion into titanium by nanosecond pulsed laser irradiation in air, Appl. Surf. Sci. 278 (2013) 245–249, http://dx.doi.org/10.1016/j.apsusc.2012.11.110.

[49] L. Lavisse, J.M. Jouvard, J.P. Gallien, P. Berger, D. Grevey, P. Naudy, The influence of laser power and repetition rate on oxygen and nitrogen insertion into titanium using pulsed nd:YAG laser irradiation, Appl. Surf. Sci. 254 (4) (2007) 916–920, http://dx.doi.org/10.1016/j.apsusc.2007.07.204.

[50] T.B. Massalski, H. Okamoto, P. Subramanian, L. Kacprzak, W.W. Scott, Binary Alloy Phase Diagrams, vol. 1(2), American society for metals Metals Park, OH, 1986.

[51] A. Sutton, Electronic Structure of Materials, Oxfrd University Press, 2004.

[52] Y.L. Hao, S.J. Li, S.Y. Sun, C.Y. Zheng, R. Yang, Elastic deformation behaviour of Ti–24Nb–4Zr–7.9Sn for biomedical applications, Acta Biomater. 3 (2) (2007) 277–286, http://dx.doi.org/10.1016/j.actbio.2006.11.002.

[53] D. Kuroda, M. Niinomi, M. Morinaga, Y. Kato, T. Yashiro, Design and mechanical properties of new β type titanium alloys for implant materials, Mater. Sci. Eng. A 243 (1) (1998) 244–249, http://dx.doi.org/10.1016/S0921-5093(97)00808-3.

[54] P. Kwasniak, F. Sun, S. Mantri, R. Banerjee, F. Prima, Polymorphic nature of 332 <113> twinning mode in BCC alloys, Mater. Res. Lett. 10 (5) (2022) 334–342, http://dx.doi.org/10.1080/21663831.2022.2049906.

[55] M. Tane, S. Akita, T. Nakano, K. Hagihara, Y. Umakoshi, M. Niinomi, H. Nakajima, Peculiar elastic behavior of Ti–Nb–Ta–Zr single crystals, Acta Mater. 56 (12) (2008) 2856–2863, http://dx.doi.org/10.1016/j.actamat.2008.02.017.

[56] M. Tane, S. Akita, T. Nakano, K. Hagihara, Y. Umakoshi, M. Niinomi, H. Mori, H. Nakajima, Low Young's modulus of Ti–Nb–Ta–Zr alloys caused by softening in shear moduli c′ and c44 near lower limit of body-centered cubic phase stability, Acta Mater. 58 (20) (2010) 6790–6798, http://dx.doi.org/10.1016/j.actamat.2010.09.007.

[57] C.K. Sudbrack, R.D. Noebe, D.N. Seidman, Direct observations of nucleation in a nondilute multicomponent alloy, Phys. Rev. B 73 (21) (2006) 1–4, http://dx.doi.org/10.1103/PhysRevB.73.212101, arXiv:0508117.

[58] M.K. Miller, E.A. Kenik, Atom probe tomography: A technique for nanoscale characterization, Microsc. Microanal. 10 (3) (2004) 336–341, http://dx.doi.org/10.1017/S1431927604040577.

[59] F. De Geuser, W. Lefebvre, D. Blavette, 3D atom probe study of solute atoms clustering during natural ageing and pre-ageing of an Al-Mg-Si alloy, Phil. Mag. Lett. 86 (4) (2006) 227–234, http://dx.doi.org/10.1080/09500830600643270.

[60] J. Zhou, J. Odqvist, M. Thuvander, P. Hedstrom, Quantitative evaluation of spinodal decomposition in Fe-Cr by atom probe tomography and radial distribution function analysis, Microsc. Microanal. 19 (2008) 665–675, http://dx.doi.org/10.1017/S1431927613000470.

[61] A. Devaraj, S. Nag, R. Srinivasan, R.E. Williams, S. Banerjee, R. Banerjee, H.L. Fraser, Experimental evidence of concurrent compositional and structural instabilities leading to ω precipitation in titanium-molybdenum alloys, Acta Mater. 60 (2) (2012) 596–609, http://dx.doi.org/10.1016/j.actamat.2011.10.008.

[62] N. Nagasako, R. Asahi, D. Isheim, D.N. Seidman, S. Kuramoto, T. Furuta, Microscopic study of gum-metal alloys: A role of trace oxygen for dislocation-free deformation, Acta Mater. 105 (2016) 347–354, http://dx.doi.org/10.1016/j.actamat.2015.12.011.